Journal of Materials Chemistry B

ROYAL SOCIETY OF CHEMISTRY

PAPER

View Article Online
View Journal

Cite this: DOI: 10.1039/c9tb02614b

H_2S-Donating trisulfide linkers confer unexpected biological behaviour to poly(ethylene glycol)–cholesteryl conjugates†

Francesca Ercole,‡[a] Yuhuan Li,‡[a] Michael R. Whittaker,[a] Thomas P. Davis*[ab] and John F. Quinn*[ac]

Inspired by the properties of the naturally occurring H_2S donor, diallyl trisulfide (DATS, extracted from garlic), the biological behaviour of trisulfide-bearing PEG-conjugates was explored. Specifically, three conjugates comprising an mPEG tail and a cholesteryl head were investigated: conjugates bridged by a trisulfide linker (**T**), a disulfide linker (**D**) or a carbamate linker (**C**), and a fourth comprising two mPEG tails bridged by a trisulfide linker (**P**). H_2S testing using both a fluorescent chemical probe in HEK293 cells and an amperometric sensor to monitor release in suspended cells, demonstrated the ability of the trisulfide conjugates, **T** and **P**, to release H_2S in the presence of cellular thiols. Cytotoxicity and cyto-protective capacity on HEK293 cells showed that **T** was the best tolerated of the conjugates studied, and remarkably more so than **D** or **C**. Moreover, it was noted that application of **T** conferred a protective effect to the cells, effectively abolishing the toxicity associated with co-administered **C**. The interaction of conjugates and combinations thereof with the cell membrane of HEK cells, as well as ROS generation were also investigated. It was found that **C** caused significant membrane perturbation, correlating with high losses in cell viability and pronounced generation of ROS, especially in the mitochondria. **T**, however, did not disturb the membrane and was able to mitigate the generation of ROS, especially in the mitochondria. The interplay of the cholesteryl group and H_2S donation for conferring cytoprotective effects was clearly demonstrated as **P** did not display the same beneficial characteristics as **T**.

Received 20th November 2019,
Accepted 19th March 2020

DOI: 10.1039/c9tb02614b

rsc.li/materials-b

Introduction

Organic polysulfides, $(R_1–(S)_n–R_2$, $n > 2)$ exist in nature in a variety of plants and fungi, primarily as molecules containing tri- and tetrasulfide bonds.[1,2] Such compounds can reveal potent antibiotic, antifungal and even anti-cancer activity, generating interest for medical and agricultural applications.[3] The health-promoting benefits provided by a diet rich in garlic and other alliums have been attributed, at least in part, to polysulfides such as diallyl trisulfide (DATS).[4,5] Studies have demonstrated the positive impacts of garlic and other alliums in mediating risk factors for cardiovascular disease, including reducing platelet aggregation and oxidative stress.[6] Some of the benefits, especially those associated with vasoactivity, are thought to be mediated by hydrogen sulfide, H_2S, an endogenous signaling molecule which elicits numerous important actions in the body (*e.g.*, relaxation of vascular smooth muscle, reduction in blood pressure).[7,8] Related impacts include gastroprotective,[9,10] cardioprotective,[11] hepatoprotective[12,13] and neuroprotective[14,15] effects. The protective effect of H_2S in the cardiovascular system has been demonstrated against damage induced by agents such as doxorubicin[16] and in the gastrointestinal system, by damage induced by non-steroidal anti-inflammatory drugs.[17] Specifically, exogenous H_2S was shown to reduce myocardial necrosis and rescue contractile activity in isoproterenol-damaged rat hearts.[18] It was also found to amend hyper-homocysteine induced myocardial tissue damage by inhibiting ER stress-associated apoptosis in rats,[19] and by eliciting a cardioprotective effect against H_2O_2-induced oxidative stress in an MI mouse model.[20] Synthetic small molecule donors have been demonstrated to protect primary H9c2 cardiomyocyte cells from hypoxia-induced injury[21] and cardiomyoblast apoptosis.[20]

[a] *ARC Centre of Excellence in Convergent Bio-Nano Science and Technology, Drug Delivery, Disposition and Dynamics Theme, Monash Institute of Pharmaceutical Sciences, Monash University, Parkville, VIC 3052, Australia. E-mail: john.f.quinn@monash.edu, thomas.p.davis@monash.edu*
[b] *Australian Institute for Bioengineering and Nanotechnology, The University of Queensland, St Lucia, Queensland 4072, Australia*
[c] *Department of Chemical Engineering, Faculty of Engineering, Monash University, Wellington Road, Clayton, Victoria 3800, Australia*

† Electronic supplementary information (ESI) available: Full synthetic details of **P**, ^{1}H NMR spectra with spectral assignments for **T**, **D**, **C** and **P**; full descriptions of all methods. See DOI: 10.1039/c9tb02614b

‡ These authors contributed equally to this work.

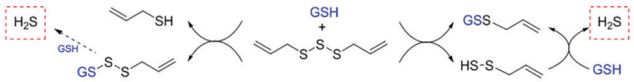

Scheme 1 Thiol exchange reaction of DATS (diallyl trisulfide) with glutathione (GSH) to generate H_2S *via* persulfide intermediates.

The possibility of applying H_2S therapeutically has motivated the development of numerous small molecule[22,23] and high molecular weight H_2S donors.[24–26] In particular, polymeric H_2S donors offer certain advantages, such as increased aqueous solubility, modulated release kinetics and the potential to tailor the pharmacokinetics of the agent.[27,28]

As shown in Scheme 1, H_2S is generated from the trisulfide DATS initially as a result of nucleophilic attack of the sulfur–sulfur bond by glutathione (GSH), to produce GSS–allyl and allyl persulfide. The persulfide (RSSH) then reacts further with GSH to produce H_2S. Alternatively, the exchange reaction results in another mixed trisulfide, GSSS–allyl, which releases H_2S in a similar fashion, *i.e.*, *via* an intermediate persulfide.[5,29,30] Notably, in a closed system the reaction between H_2S and an oxidized thiol, RSSR, can also occur, to generate a persulfide[31] in equilibrium with all the species, H_2S, RSH, RSSR, RSSH and RSSSR.[32] Persulfide generation on critical protein cysteines constitutes a post-translational modification and a mechanism by which H_2S is thought to signal.[33,34] The emerging role of persulfide species as possible mediators of H_2S signaling and their biochemistry is of increasing interest and scrutiny.[35–37]

Our interest is in nanomaterials incorporating polysulfide bonds, with an emphasis on their ability to generate H_2S and biological benefits thereof. In a previous communication[38] we described the synthesis and physical properties of a polymeric conjugate incorporating a trisulfide linkage, bridging hydrophilic and hydrophobic sections. The mPEG-SSS-cholesteryl conjugate known as **T**, was shown to be capable of self-assembling into micelles and to biodegrade in a cellular environment to concurrently deliver H_2S. In this work we delve further by focusing our attention on probing the activity of **T** in a biological environment. Namely, we carry out cellular *in vitro* assays investigating cytotoxicity, ROS mitigation, membrane effects and H_2S donation. As previously, we apply the controls, **D**, a disulfide version which is also capable of exchanging with thiols (but without concomitant release of H_2S) and a non-cleavable, non H_2S-donating version, **C**. In this study we include another control, **P**, an H_2S-donating, water-soluble version, incorporating a trisulfide bridge yet no lipid tail. The comprehensive study presented here builds a more complete picture regarding activity of **T**, beyond physical properties which were probed in the initial publication. Importantly, the biological tests conducted here give a better understanding of designed trisulfide nanomaterials which is a necessary step towards realizing their potential to be applied in a pharmaceutical setting.

Experimental

Materials

Cholesteryl (((2-methoxyPEGamino)carbonyloxyethyl)trisulfan-yl-ethyl)carbamate (**T**), cholesteryl (((2-methoxyPEGamino)carbonyl-oxyethyl)disulfanylethyl)carbamate (**D**), cholesteryl-PEG-OMe carbamate (**C**) were synthesized as previously described,[38] (ESI,† Schemes S1–S3 and ^{1}H NMR Fig. S1–S3). MeO-PEG-SSS-OMe (**P**) was synthesised using a different method for the generation of the trisulfide bridge[39] (ESI† synthetic protocol, Scheme S4 and ^{1}H NMR Fig. S4). The fluorescent probe for H_2S detection in cells, SF4, was synthesized as described.[40]

MeO-PEG-NH_2 MW 2000 g mol^{-1} (Linear Monofunctional PEG Amine NH_2) was purchased from Creative PEGWorks. Sodium sulfide (Na_2S) anhydrous was purchased from Alfa Aesar and hydrochloric acid 32% was purchased from Ajax FineChem. Solvents (except anhydrous solvents) were purchased from Merck Millipore and used as received. All other chemicals, such as reagents and anhydrous solvents for synthesis, were purchased from Sigma-Aldrich at the highest purity available and used without further purification (unless otherwise stated). A Reveleris Flash Chromatography System fitted with silica gel (230–400 mesh) cartridges was used for purification of monomer and intermediates. TLC was performed on Merck Silica 60F254 plates. PBS 7.4 (phosphate buffered saline, pH 7.4) was reconstituted from powder (Sigma-Aldrich) which, when dissolved in 1 L of deionized water, yielding 0.01 M phosphate buffered saline (NaCl 0.138 M, KCl 0.0027 M), pH 7.4 at 25 °C.

Characterization and methods

^{1}H (400 MHz) and ^{13}C NMR (100 MHz) spectroscopy. Spectra were obtained with a Bruker UltraShield 400 MHz spectrometer at 25 °C running Bruker Topspin Software. Spectra were recorded for samples dissolved in deuterated solvent and chemical shifts are reported as parts per million from external tetramethylsilane.

CMC determination. 990 μL of 13 different polymer solutions of decreasing concentration (1.0 to 0.000001 mg mL^{-1}) were added individually to 13 vials. These are prepared by diluting a 5.0 mg mL^{-1} polymer stock solution with MilliQ water. A pyrene stock solution ($c = 5 \times 10^{-5}$ M) was prepared in THF and 10 μL aliquots were added to the 13 vials containing the polymer solutions. The final pyrene concentration in each vial was 5×10^{-7} M. Vials were shaken gently for two hours at room temperature, shielded from the light with aluminium foil. The fluorescence spectra were recorded using an excitation wavelength of 336 nm and emission spectra were recorded ranging from 350 to 450 nm. From the pyrene emission spectra, the intensities (peak height) of the 393 nm peak (I_1) and 384 nm peak (I_3) were used to calculate the I_3/I_1 ratio.

A CMC value was determined from plots of log C *vs.* pyrene I_3/I_1 ratio by fitting the curves to a Boltzmann sigmoid type equation[41] given by:

$$y = \frac{A_1 - A_2}{1 + e^{(x - x_0)/\Delta x}} + A_2$$

where y corresponds to the pyrene I_3/I_1 ratio value; the independent variable (x) is the concentration of polymer; A_1 and A_2 are the upper and lower limits of the sigmoid respectively; x_0 is the centre of the sigmoid and Δx is directly related to the independent variable (x) range where there is an abrupt change of the dependent (y) variable. A CMC value (CMC_1) was taken to be,

x_0 the centre of the sigmoid, as determined using KaleidaGraph curve fitting software for the series of data points.

Glutathione-mediated H_2S release from the conjugates T and P in cell media as measured using the amperometric sensor. Polymeric solutions of **P** and **T** were prepared in Milli Q water to a final polymer concentration of 7.2 mg mL^{-1} and 5 mg mL^{-1} respectively. The sensor tip was immersed into a vial containing cell culture media only (Dulbecco's Modified Eagle Media, DMEM, high glucose, Sigma-Aldrich, supplemented with 10% (v/v) Fetal Bovine Serum, FBS) (500 μL) for the first 10 minutes, then **P** (50 μL of 7.2 mg mL^{-1} stock solution, 8.2×10^{-8} moles) or **T** (50 μL aliquot of 5 mg mL^{-1} stock solution, 8.2×10^{-8} moles) is added. As with the calibration, in order to minimize exposure to air and loss of H_2S to the environment, Parafilm was used to cover the mixture during the measurements. During the measurements the mixture was stirred with a magnetic stirrer bar. H_2S release was monitored for a period of 10–12 minutes. Glutathione (GSH) was then injected into the stirring solution using a micro-syringe (20 μL of a 250 mM solution in water, 5.0×10^{-7} moles) and then H_2S release was monitored for another period of 20–25 minutes. For each release curve over time, the peaking $[H_2S]$ and the corresponding peaking $[sulfides]_{tot}$ was calculated and displayed, as derived from the calibration plot (refer to ESI† for calculations, as well as previous work[42]).

Cell culture. HEK 293 (Human embryonic kidney cells, ATCC) were grown in DMEM supplemented with 10% FBS. Cells were cultured at 37 °C in a humidified incubator with 5% atmospheric CO_2.

Cell-mediated H_2S release from the conjugates, T and P, as measured using the amperometric sensor. HEK293 (cultured as described above and maintained in T75 flasks) were detached with trypsin, isolated as a plug, re-dispersed in complete media and then counted. Two individual groups of equal volume and cell concentration were dispensed in separate vials. The sensor was immersed in each cell population, a signal was measured (for approx. 2 minutes) and then a **T** or **P** aliquot was added: 50 μL, 5 mg mL^{-1} stock solution, 8.2×10^{-8} moles for **T**, and 50 μL, 7.2 mg mL^{-1} stock solution, 8.2×10^{-8} moles for **P**. For each release curve over time, the peaking $[H_2S]$ and the corresponding peaking $[sulfides]_{tot}$ was calculated and displayed, as derived from the calibration plot (refer to ESI† for calculations, as well as previous work[42]).

Alamar blue assay. All assay plates were coated with poly-L-lysine solution (mol wt 150 000–300 000, 0.01%, sterile-filtered, BioReagent). HEK293 cells (cultured as described above) were seeded in a 96-well plate (1.5×10^4 cells per well) in the cell medium overnight and subsequently incubated with serial dilutions of polymer samples (1000, 500, 250, 125, 63 and 31 μg mL^{-1} for **T**, **C** and **D**) and (1440, 720, 360, 180, 90 and 45 μg mL^{-1} for **P**) made up in cell culture medium containing 1% (v/v) antibiotic (penicillin–streptomycin solution), for 24 h at 37 °C and with 5% CO_2. Cell culture medium containing 1% (v/v) antibiotic was used as a control. Each polymer was tested in triplicate at each concentration to obtain representative cell viability values. After exposure of cells to polymer samples the media was removed, and cells were incubated with 10% v/v AlamarBlue™ Cell Viability Reagent (ThermoFisher) in cell culture media containing 1% (v/v) antibiotic, for 4 h at 37 °C and 5% CO_2. A microplate reader (CLARIOstar, BMG LABTECH) was used to read the fluorescence at 560 nm excitation and 590 nm emission. Background values (10% AlamarBlue in cell culture medium with 1% (v/v) antibiotic, with no cells) were subtracted from each well and the average fluorescence intensity of the triplicates was calculated.

Cell based high-content SF4 time-course study. Solutions of polymers were made to a final concentration of 1 mg mL^{-1} for **T** and 1.4 mg mL^{-1} for **P**. The solutions were then diluted 1:10 in PBS 7.4 prior to addition to the cells (final concentration 0.1 mg mL^{-1} for **T** and 0.14 mg mL^{-1} for **P**). The solutions of SF4 were prepared fresh in DMF/DMSO (5 mM) and diluted to give a 5 μM solution in Hank's Balanced Salt Solution (HBSS).

HEK293 cells (1.5×10^4 cells per well) were seeded in black, optically clear 96-well plates and grown to 90% confluency. Cells were washed with HBSS, then loaded with 5 μM SF4 probe (in 90 μL HBSS) for 10 minutes at 37 °C. Fluorescence imaging was performed using a high-content PerkinElmer Operetta with an Olympus LUCPlanFLN 20× (NA 0.45) objective. SF4 fluorescence was visualized using the EGFP filter set (excitation 460–490 nm, emission 500–550 nm). Images were taken every 4 minutes. After baseline fluorescence was determined for 8 minutes, the polymeric solution (10 μL) was added into wells, then images were taken every 4 minutes for 1 hour at 37 °C. After that, images were taken every 1 hour for 23 hours at 37 °C. Data were automatically analyzed by determining the mean SF4 fluorescence per well using Harmony High Content Imaging and Analysis software (v3.5.2). SF4 fluorescence was PBS vehicle subtracted and expressed relative to the baseline fluorescence for each experimental condition. Data are expressed as the mean ± SD from three independent experiments.

ROS detection

HEK293 cells (1.5×10^4 cells per well) were exposed to materials for 1, 2 and 4 hours in 96-well plates. Cell culture medium was used as a control. The CellROX™ Deep Red Reagent was added to the cells at a final concentration of 10 μM followed by incubation for 40 minutes at 37 °C. The medium was then removed, and the cells were washed three times with PBS. Fluorescence imaging was performed using a high-content PerkinElmer Operetta with an Olympus LUCPlanFLN 20× (NA 0.45) objective. The fluorescence was visualized using the mCherry filter set (excitation 640 nm, emission 665 nm). Background values (PBS only) were subtracted from each well and the average fluorescent intensity of the triplicates was calculated.

MitoSOX (mitochondrial superoxide indicator) test

HEK293 cells (4.0×10^4 cells per well) were seeded in 8 well chamber and cultured overnight. Cells were washed with HBSS, then loaded with 2.5 μM MitoSOX™ Red Mitochondrial Superoxide Indicator, in 300 μL HBSS for 30 minutes at 37 °C and the plates were kept protected from light. Cells were washed gently

three times with warm HBSS buffer, then stained with Hoechst 33342 stain for 1 minute, followed by imaging.

PI staining experiment

HEK293 cells (3.0×10^4 cells per well) were seeded in 8 well chamber and cultured overnight. Cells were washed with HBSS, then loaded with **C**, **D**, **T** and **P** combinations (**T** 500 μg mL^{-1}; **C** 31.25 μg mL^{-1}; **D** 125 μg mL^{-1}; **P** 720 μg mL^{-1}) for 24 hours at 37 °C. After that, PI was added into the wells at a final concentration of 1 μM for 30 minutes, and then imaging was started.

Ratiometric imaging

HEK293 cells (1.5×10^4 cells per well) were seeded in 8 well chamber coated with poly-D-lysine and cultured overnight. Prior to imaging, old media was removed and replaced with serum-free Opti-MEM (Life Technologies), with cells washed in between using Opti-MEM. Laurdan dye was added to each well to a final concentration of 5 μM and allowed to equilibrate with the cell membranes for at least 30 minutes. Cells were transferred to a Leica SP8 inverted confocal fluorescence microscope housed in a humidified, 37 °C, 5% CO_2 environment. Appropriate areas of each well, containing at least 10 viable cells, were identified. **C**, **D**, **T** and **P** (**T** 500 μg mL^{-1}; **C** 31.25 μg mL^{-1}; **D** 125 μg mL^{-1}; **P** 720 μg mL^{-1}) and combinations thereof were added to respective wells. Imaging was undertaken at 0 minutes (*i.e.* before adding the material) and at 20 minutes timepoints with a 40× oil objective. Laurdan dye integrated into cell membranes was excited along the 405 nm laser line and emission read at 430–470 nm (representing the lipid membrane at the gel/liquid ordered phase) or 480–550 nm (representing the lipid membrane at the liquid disordered phase). To calibrate dye background levels, a well containing dye only was excited on the 405 nm laser line using 0.5 and 2× laser power. Images were false-coloured and any adjustments made using LAS X software (Leica).

Determination of generalised polarization (GP)

The acquisition of GP images was performed using the ImageJ (National Institute of Health) software and custom-written macro by Owen *et al.*[43] with some modifications. GP values were then calculated for each pixel of a cell membrane according to the following equation:

$$\mathrm{GP} = \frac{I_{400-460} - I_{470-530}}{I_{400-460} + I_{470-530}}$$

where I represents the intensity of pixels in the areas of interest in the image acquired in the ordered (430–470 nm) and disordered (480–550 nm) spectral channels. The GP shift was observed by subtraction of the GP distribution peak maximum of each sample with 20 minutes of incubation time from the GP value of the image taken at the beginning of the experiment (at 0 minutes).

Results and discussion

The polymeric constructs, **T**, **D** and **C**, shown in Fig. 1, were synthesized as previously described (ESI,† Schemes S1–S3).[38]

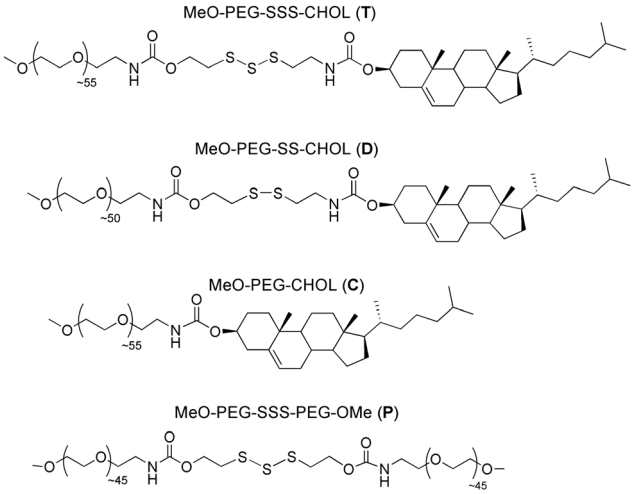

Fig. 1 OMe-PEG–(S)n–CHOL and OMe-PEG-(S)3-PEG-MeO conjugates investigated in the study (n = 0, 2 or 3).

A commonality between each is a hydrophilic PEG tail and a hydrophobic cholesteryl moiety. However, **C** does not contain a degradable bridge between both sections. The water-soluble construct **P**, which incorporates a trisulfide bridge yet no cholesteryl tail, was also synthesized as part of this study to elucidate any effects of the cholesteryl tail. The reaction of a trisulfide bridge with intracellular thiols not only imparts cleavability to the synthetic conjugate, but also enables the delivery of H_2S, both of which could be of interest in a pharmaceutical setting.

In our previous work, we demonstrated, using Nile Red as both the cargo and probe, that micelles composed of **T** could be disassembled using the thiol, L-cysteine, as a result of cleavage of the trisulfide bridge. We also demonstrated that this was concurrent with release of H_2S. Herein, we demonstrate that in a biological setting the trisulfide carriers are also able to undergo thiol-stimulated cleavage to deliver H_2S. We applied the fluorescent probe for H_2S detection, SF4,[40] which undergoes reduction of its azides into amines by H_2S, to ascertain that both **T** and **P** are capable of donation in a cellular environment. The fluorescence was measured over time in HEK293 cells which had been incubated with either **T** or **P** along with SF4 probe, without the addition of exogenous thiols. As can be seen in Fig. 2 (showing the average fluorescence result) both trisulfide donors caused a change in fluorescence over time, demonstrating their ability to donate H_2S to live cells *via* reaction with endogenous thiols. The representative fluorescent images are displayed in ESI† (Fig. S5).

The H_2S-donating ability of **T** and **P** was further demonstrated in a cellular environment using amperometry. In this method, an amperometric microsensor (Unisense) was immersed in cell media (DMEM with 10% FBS) containing cultured HEK293 cells of known concentration. The cells were previously detached and re-suspended in fresh media prior to measurement. During the measurement the cells were gently stirred in the media to reduce sedimentation. Given that cells may have become compromised during the test, it was stopped at 60 minutes with further testing

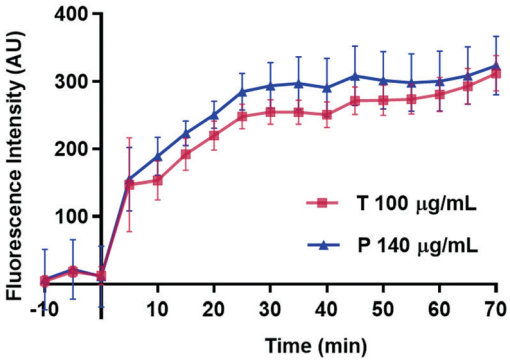

Fig. 2 Fluorescence intensity of SF4 probe over time in HEK293 cells on addition of MeOPEG-SSS-CHOL (**T**) and MeOPEG-SSS-PEGOMe (**P**). SF4 fluorescence is PBS-vehicle subtracted.

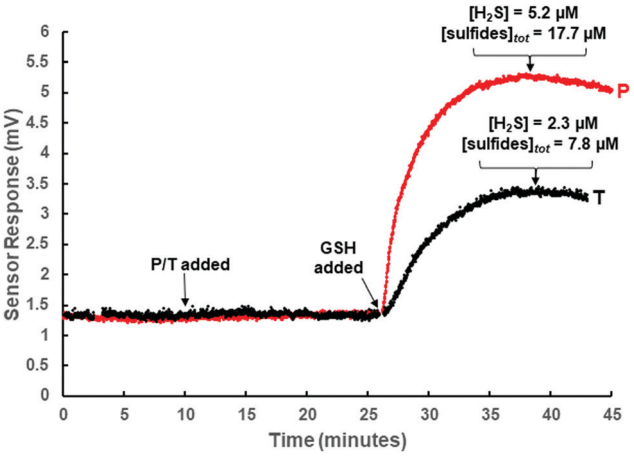

Fig. 3 Representative H_2S release curve for **P** (red) and **T** (black) in cell culture medium (Dulbecco's Modified Eagle Media, DMEM) with (10% Fetal Bovine Serum, FBS), as measured using amperometric microsensor (Unisense). Note: the first 10 minutes is measured in cell culture media only, then **P** (50 μL of 7.2 mg mL^{-1} solution in water added, 8.2×10^{-8} moles) or **T** (50 μL aliquot of 5 mg mL^{-1} solution in water is added, 8.2×10^{-8} moles) is added. Glutathione (GSH) is then added where indicated (20 μL of a 250 mM solution in water, 5.0×10^{-7} moles). The values for peaking $[H_2S]$ and peaking $[sulphides]_{tot}$ shown are derived from calibration plot.

unlikely to be meaningful. ESI,† Fig. S6 displays the individual release profiles of **T** and **P** in three cell populations, with graphs in the top row (a1–c1) representing release from cells exposed to **T** and graphs in the bottom row (a2–c2) representing release profiles from cells exposed to **P**. In this test the extracellular H_2S was detected, however we cannot determine whether this involves trisulfides being taken up by the cells, to react with intracellular thiols, or whether thiols existing in the extracellular space are reacting with the trisulfides to generate H_2S. Notably, however, no exogenous thiols were added indicating that both **T** and **P** are capable of donating H_2S to cells *via* reaction with endogenous thiols. This is in line with our previous cellular tests using SF4. Furthermore, since H_2S was detected only after the addition of both **T** and **P** conjugates to cells and media, this means that the sensor was not simply detecting endogenous H_2S production by the cells. Therefore, it was established qualitatively using the amperometric method, that both trisulfide conjugates, **T** and **P**, can generate H_2S *via* their reaction with cellular thiols.

We also explored the reactivity of the trisulfides with cell culture medium only, as well as with glutathione (GSH), a biologically relevant thiol which exists in the intracellular environment. Amperometry was again used to measure the release of H_2S, as shown in Fig. 3, which is a representative curve (refer to Fig. S7, ESI,† for subsequent run). In cell culture media alone, there was no release when both **P** and **T** were added, however when GSH was added ($\sim$6 equivalents *vs.* **T**/**P**), H_2S was generated immediately. At face value it appears that the release from **P** is higher compared to **T**, however more tests would be required in order to draw any quantitative conclusions regarding release capacity.

To demonstrate the suitability of the trisulfide conjugates for biomedical application, we tested the dose-dependent effects on cell viability. All constructs were evaluated against the HEK 293 (human embryonic kidney) cell line using Alamar Blue assay. Cell viability was tested after 24 hours of exposure of cells to each conjugate. Results, displayed in Fig. 4a–c, show a striking disparity in viability results between **T**, **D** and **C**, with **T** showing negligible cytotoxicity at concentrations up to 1000 μg mL^{-1} (0.33 mM) and **C** showing the highest dose-dependent toxicity profile. The cell viability assay was also conducted using lower doses of **C** (ESI,† Fig. S8) which showed a sharp decrease in cell viability occurs at concentrations >15 μg mL^{-1}. It is also important to understand the influence of chemical structure on toxic or cell-protective effects. For this reason, we also tested the impact on cell viability of the water-soluble construct **P** which incorporates a trisulfide bridge, yet no cholesteryl tail (Fig. 4d). Since **P** is still capable of releasing H_2S, any associated influence of the cholesteryl tail on viability may also become evident. Due to having two conjugated PEG tails, the molecular weight of construct **P** (4400 g mol^{-1}) is higher than **C**, **D** and **T** and

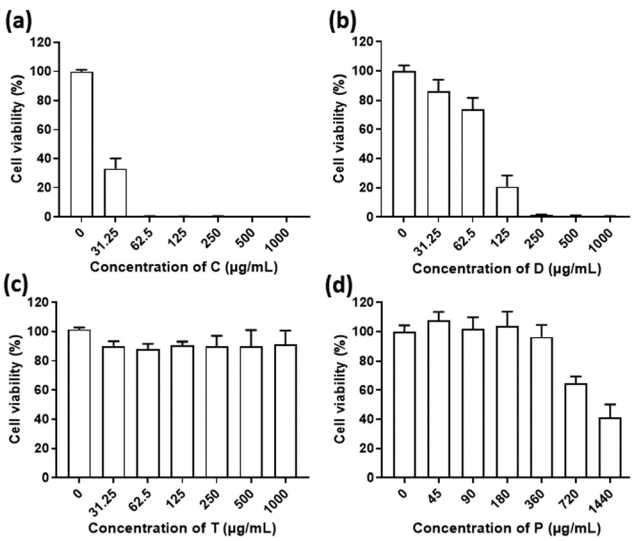

Fig. 4 Cytotoxicity evaluation of (a) MeO-PEG-CHOL, **C** (b) MeO-PEG-SS-CHOL, **D** (c) MeO-PEG-SSS-CHOL, **T** and (d) MeO-PEG-SSS-PEG-OMe, **P** conjugates against HEK-293 cells, as determined by Alamar Blue assay after 24 hours of exposure of cells to conjugates.

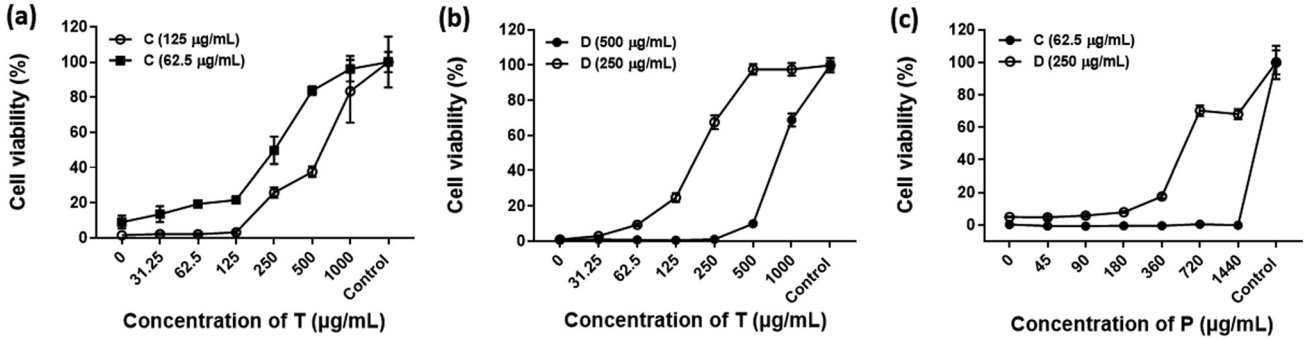

Fig. 5 (a) Protective effect of **T** on **C**-induced cytotoxicity in HEK293 cells. Cell were exposed to increasing concentrations of **T** along with two different toxic doses of **C** (125 μg mL^{-1} and 62.5 μg mL^{-1}) for 24 hours and subjected to Alamar Blue cell viability assay. Control group is without **T** and **C** and "0" point refers to **C** only (without **T**); (b) protective effect of **T** on **D**-induced cytotoxicity in HEK293 cells. Cells were exposed to increasing concentrations of **T** along with two different toxic doses of **D** (250 μg mL^{-1} and 500 μg mL^{-1}) for 24 hours and subjected to Alamar Blue cell viability assay. Control group is without **T** and **D** and "0" point refers to **D** only (without **T**); (c) protective effect of **P** on **C** and **D**-induced cytotoxicity in HEK293 cells. Cells were exposed to increasing concentrations of **P** along with two different toxic doses of **C** (62.5 μg mL^{-1}) and **D** (250 μg mL^{-1}) for 24 h and subjected to Alamar Blue cell viability assay. Control group is without **P** and **C** and **D** and "0" point refers to **C** or **D** only (without **P**).

therefore the concentrations were tested up to 1440 μg mL^{-1} (0.33 mM). **P** was found to be well tolerated by HEK cells, although marginally less so than **T**. These results therefore suggest some interplay between toxicity and the cholesteryl tail.

An investigation into the cyto-protective capacity of the H_2S-donors, **T** and **P**, was also conducted. This was assessed by undertaking a cell rescue test using an Alamar Blue cell viability assay. In this investigation the **T** or **P**-dose dependent effect on viability was screened when HEK cells were co-incubated (for 24 hours) with an otherwise toxic dose of **C** (either 62.5 or 125 μg mL^{-1}) and **D** (either 250 μg mL^{-1} or 500 μg mL^{-1}). As shown in Fig. 5a, on increasing the **T** concentration from 31.25 to 1000 μg mL^{-1} for an exposure time of 24 hours, the protective effect of **T** against **C**-induced cytotoxicity was found to increase in a dose-dependent manner. The same effect of **T** was demonstrated on **D**-induced cytotoxicity (Fig. 5b). However, for **P**, a protective effect was only demonstrated against **D**, with **C**-induced cytotoxicity not able to be diminished across all doses of **P** (Fig. 5c).

The minimum concentration of **T** or **P** required to affect an improvement in viability to 50%, *vs.* the '0' control group (*i.e.*, with no **T** or **P** present), was estimated for each group as displayed in Table 1. As expected, the higher the dose of **C** or **D** that the cells were exposed to, the higher the concentration of **T** or **P** that was required to rescue the cells. It is also notable that **T** is an effective cell protector against **C**, however **P** is completely ineffective. This result indicates that the cholesteryl group likely has an important role in the cyto-protection, and that H_2S is not solely responsible for this effect.

Further experiments, aimed at elucidating the mechanism by which **T** protects HEK cells from **C**/**D**-induced toxicity, led us to investigate their effects on membrane integrity. Propidium iodide (PI) is a useful dye for such purposes since it binds to double-stranded DNA but cannot cross an intact plasma membrane. Therefore, it will only be present in the DNA of cells which have had their plasma membranes compromised and permeabilized. In this study HEK293 cells were loaded with **C**, **D**, **T** and **P** combinations for 24 hours, after which time PI was added for 30 minutes before imaging (Fig. 6). The doses of **C** (31.25 μg mL^{-1}) and **D** (125 μg mL^{-1}) chosen for the combinations with **T** and **P** were lower than the previous experiment to maintain a higher population of cells for imaging.

Table 1 Protective effect of **T** and **P** on cell viability in the presence of **C** and **D**, as assessed by Alamar Blue assay

Co-incubation groups	Concentration of **T**/**P** at which 50% of cells remain viable (μg mL^{-1})
T + **C** (62.5 μg mL^{-1})	250
T + **C** (125 μg mL^{-1})	640
T + **D** (250 μg mL^{-1})	200
T + **D** (500 μg mL^{-1})	890
P + **C** (62.5 μg mL^{-1})	—
P + **D** (250 μg mL^{-1})	590

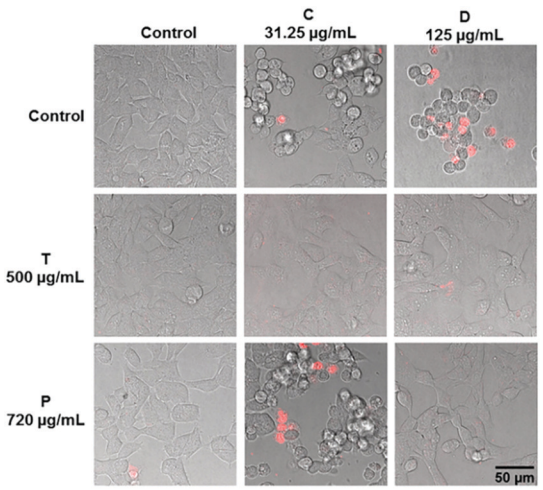

Fig. 6 Propidium Iodide (PI) detection in HEK293 cells exposed to combinations of: **T** (500 μg mL^{-1}) and **C** (31.25 μg mL^{-1}); **T** (500 μg mL^{-1}) and **D** (125 μg mL^{-1}); **P** (720 μg mL^{-1}) and **C** (31.25 μg mL^{-1}); and **P** (720 μg mL^{-1}) and **D** (125 μg mL^{-1}). Merged Confocal Microscope images.

Fig. 6 shows a moderate infiltration of PI in the **D**-only images and a small amount into the **C**-only sample. Both **D**-only and **C**-only images have a high number of round cells that have departed from their normal cell morphology. However, comparing these results to the cell viability results (Fig. 4), it is reasonable to conclude that necrosis by loss of membrane integrity does not fully account for toxicity effects, especially for **C**. Both **T**-only and **P**-only images show no evidence of infiltration, and preservation of normal cell morphology, in line with their cell viability results which showed high viability of cells maintained even at high doses. The **P–C** combination image in Fig. 6 shows moderate infiltration of PI and a high incidence of round cells, in contrast to the **P–D** combination image, in which cells are uncompromised. These distinct results are in line with the previous cell rescue tests (Fig. 5c) which showed that **P** could rescue **D**-exposed cells but was unable to rescue cells exposed to **C**.

This difference likely arises from the degradability of **P** and the interaction of the degradation products with **D**. As mentioned previously,[32,35–37] an important reaction studied in literature, partly due to its significance to post-translational modification of proteins, is the reaction of H_2S with oxidized thiol derivatives to generate a persulfide (R-SSH), as in:

$$H_2S + RSSR \rightleftarrows RSSH + RSH$$

As such, there is the potential for H_2S generated from **P** to react with the disulfide bridge of **D**, resulting in a loss of its amphiphilic structure. This could result in a diminished or less harmful interaction with the cell membrane. With a range of products generated from the GSH-mediated cleavage of trisulfides, **P** and **T**, such as, H_2S, RSH, RSSR, RSSH and RSSSR (ESI,† Fig. S9), the ongoing reaction of H_2S with **D** could produce persulfides such as CHOL-SSH, which could be pertinent mediators involved in protection. Importantly, CHOL-SSH would only be produced in combinations where cyto-protection is observed, but this would not be the case for the **P–C** combination.

Cell membrane destabilization and/or destruction are events that could take place when a surfactant comes into contact with cells and these events can be influenced by their self-assembly behaviour.[44] The degradability of the conjugate (which would be the case for **T** and **D**) and loss of amphiphilicity in a cellular environment could also be associated factors to consider with respect to plasma membrane interactions and toxic effects. Indeed, studies on amphiphilic, non-ionic surfactants such as Triton and Tween series have shown that surfactants can integrate-with and even solubilise lipid membrane components, depending on concentration and surfactant structure. Specifically, the toxicity of non-ionic surfactants to HeLa cells were found to increase with increasing chain length of the hydrophobic tail. Additionally, toxic doses were found to exist above the critical micelle concentration (CMC) of the surfactants evaluated in these studies.[46,47] This would suggest that a strong tendency to self-assemble, may also increase the likelihood of a surfactant to destabilize the cell membrane. We therefore determined the CMC of the conjugates, which

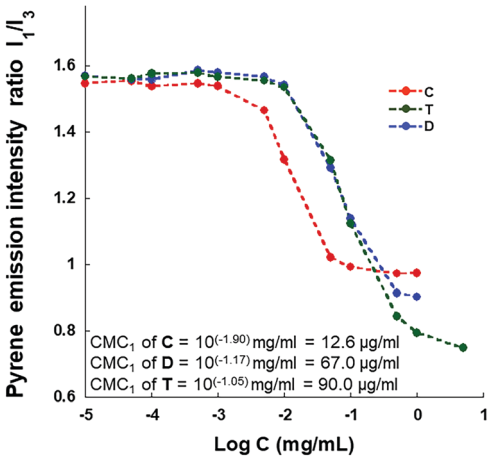

Fig. 7 Plots of pyrene 1 : 3 ratio *versus* concentration of **C**, **T** and **D** in Milli Q water, experimental data were fitted by a decreasing sigmoid of the Boltzmann type to derive CMC_1, taken to be the critical micelle concentration.

self-assemble into micelles in aqueous solution. The determination of the CMC for each conjugate was carried out by the pyrene 1 : 3 ratio method.[41] Briefly, a plot of the pyrene fluorescence intensity ratio (I_1/I_3, measured at the wavelengths corresponding to the bands located near 373 and 384 nm) as a function of the total surfactant concentration, displays around the CMC, a sigmoidal decrease. Below the CMC, the pyrene 1 : 3 ratio value corresponds to a polar environment, and as the surfactant concentration increases, the pyrene 1 : 3 ratio decreases rapidly to indicate that the pyrene is sensing a more hydrophobic environment. Above the CMC, the pyrene 1 : 3 ratio reaches a roughly constant value because of the incorporation of the probe into the hydrophobic region of the micelles.

As displayed in Fig. 7 (and ESI,† Table S1), the CMC value of conjugate **C** ($\sim$13 μg mL^{-1}) was found to be well below that of **T** and **D**, and also to be closest in value to the concentration range at which it displays toxicity ($>$15 μg mL^{-1}). This is in line with studies conducted on HeLa cells using non-ionic surfactants in which they were found to be more toxic above or close to their CMC values.[45] For **D** and **T**, which carry either two or three successive sulfur atoms in their structures, the CMC values were found to be significantly higher (67 and 90 μg mL^{-1}). This would be expected, as sulfur is much larger than carbon and oxygen and multiple sulfurs are likely to affect the packing-ability and stability of the self-assembled system. However, since **D** and **T** degrade to lose their surfactant structure, the interplay of their degraded structures with the membrane are also important considerations. The degradability of **D** in a cellular environment may explain the higher cell viability results compared to **C**. However, it is notable that its measured CMC value (67 μg mL^{-1}) was also found to occur relatively close to its toxic concentration range ($>$62.5 μg mL^{-1}).

It has been demonstrated in literature that non-ionic surfactants can induce apoptosis by way of insertion into the cell membrane, and that this process can occur at low surfactant concentrations. Membrane insertion can trigger an apoptotic

signal inside the cell by way of transduction. At higher concentrations the disruption of the cell membrane can occur *via* mixed micelle formation between surfactant and membrane phospholipids, leading to cell necrosis (known as a detergent effect).[47]

Membrane damage *via* a detergent effect, with subsequent permeabilization does not account for the toxic effect of **C** since this was not demonstrated by the PI test. However, a physical association between the cholesteryl conjugate and the cell membrane, such as membrane insertion, is conceivable as has been demonstrated for other cholesteryl-based self-assemblies.[48] Such events could potentially activate a pathway that co-elicits a cytotoxic effect.[49] We therefore applied the lipophilic dye, 6-dodecanoyl-2-dimethylaminonaphthalene (Laurdan), to probe the physical association of the conjugates on membrane lipid order.[43,50] We investigated the interaction of all conjugates and combinations thereof with the cell membrane of HEK cells using ratiometric imaging. The lipophilic Laurdan dye undergoes spectral red-shifting upon an increase in membrane fluidity, thus acting as a reporter for cell membrane lipid order. Changes in cell membrane lipid order, namely between the gel/liquid ordered phase (I_0, predominantly fluorescent at 430–470 nm) and the liquid disordered phase (I_d, predominantly fluorescent at 480–550 nm), were determined by generalised polarisation, GP, (see ESI† for methodology), where a negative GP shift indicates decreased membrane lipid order, *i.e.*, pertubation.[51]

As can be seen in Fig. 8, membrane lipid order did not change in control cells (no conjugate added), nor when cells were incubated with **T**. The largest GP shift occurred with **C** (GP shift = −0.12), followed by **P** (−0.059) and **D** (−0.049). Notably, at 20 minutes, the morphology of the cells exposed to **C** showed an unhealthy, rounded appearance (Fig. 9, left panels), as was observed for **D**-exposed and **P**-exposed cells. When **C** was combined with **T**, the GP shift reduced significantly (from −0.12 to −0.012), as was seen, although to a lesser extent, for the **D** and **T** combination (Fig. 9). These results indicate that membrane perturbation may be involved with toxic effects and subsequent cell death.

The specific mechanism for **C**-induced toxicity and **T**-induced protection is still uncertain, however, one possibility is that it involves reactive oxygen species, ROS, which are known to contribute to cell dysfunction. We therefore sought to investigate ROS generation in HEK cells incubated with the conjugates **C**, **D**, **T** and **P** and then determined whether ROS production or mitigation correlated with cell viability results. This was analysed using the fluorogenic dye, CellROX™ Deep Red Reagent. The cell-permeant dye is non-fluorescent while in a reduced state and exhibits bright fluorescence upon oxidation

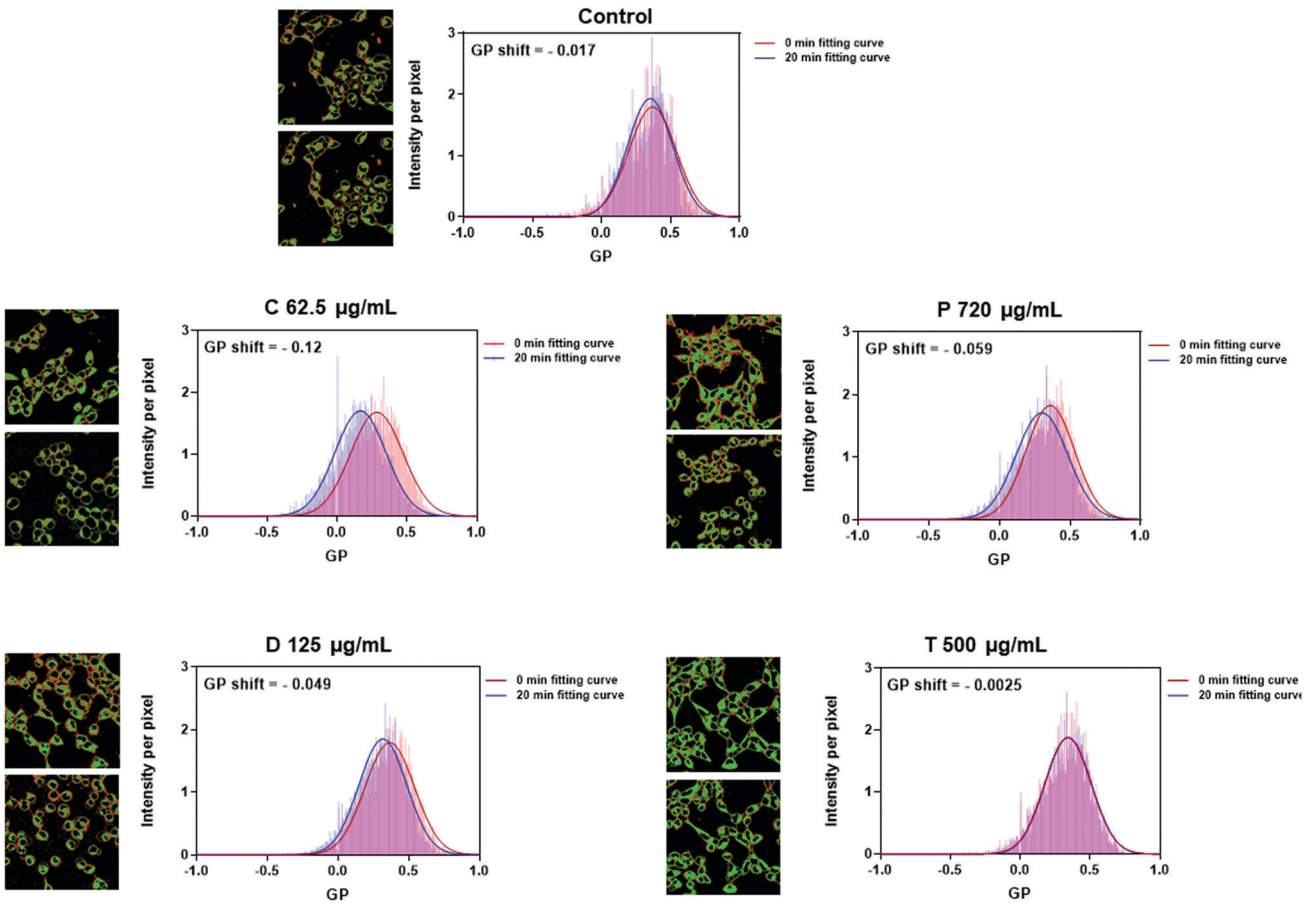

Fig. 8 Ratiometric imaging of HEK293 cells treated for 20 minutes with **T** (500 µg mL^{-1}); **C** (62 µg mL^{-1}); **D** (125 µg mL^{-1}) and **P** (720 µg mL^{-1}). The shift in GP values for HEK cells labelled with Laurden dye was recorded for 20 minutes.

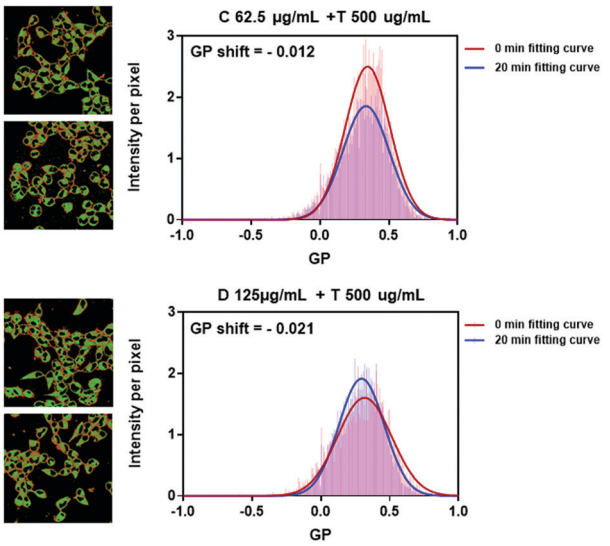

Fig. 9 Ratiometric imaging of HEK293 cells treated for 20 minutes with combinations: **T** (500 µg mL^{-1}) and **C** (62.5 µg mL^{-1}) and **D** (125 µg mL^{-1}) and **T** (500 µg mL^{-1}) combinations. The shift in GP values for HEK cells labelled with Laurden dye was recorded for 20 minutes.

by reactive oxygen species. Initially, low doses of **C**, **D** and **T** were tested (31.25 µg mL^{-1}), as in Fig. 10 (left panel). Conjugates **C** and **D** caused an increase in ROS, even at low concentration, whilst **T** caused a small drop in ROS from basal levels after 4 hours. Higher doses of **T** and **C** were tested, along with the other H_2S donor, **P**, with results shown in Fig. 10 (right panel). **P** was found to be ineffectual in reducing ROS, whilst **T** caused a significant drop compared to the control. Taken together, these results suggest that it is a combination of cholesteryl group and H_2S that is involved in the eliciting a ROS-mitigating effect. Notably, there is a significant reduction in ROS when **T** was combined with **C**, that is a reduction of ~50% compared to **C** alone and ~25% reduction compared to the control group.

Given that the ROS results are well correlated with toxicity, it is likely that ROS production plays a role in **C**-mediated toxicity and that the cyto-protective effect of **T** (on **C**) involves the mitigation of ROS. That is, when **T** was combined with **C**, toxicity was reduced, as was ROS. These related effects are also likely to involve interactions with the membrane, since results of membrane perturbation tests were well correlated with both toxicity and ROS generation. Specifically, association of **C** with the cell membrane caused the largest GP shift and induced the highest levels of oxidative stress in cells, as well as cell death. Furthermore, combination of **T** with **C** caused a significant reduction of membrane perturbation, compared to what was seen for **C** alone. Whilst **P** is a potent donor, able to generate H_2S in the presence of cellular thiols, its activity did not match that of **T**. Viability of HEK cells remained high in the presence of high concentrations of **P**, however, it did not adequately protect cells in the presence of **C**, nor mitigate the production of ROS. Furthermore, **P** caused some membrane disturbances, albeit only to a minimal level compared to control group. It is reasonable to suggest an interplay of H_2S and cholesteryl group is necessary for protection.

Mitochondria are a major source of ROS, such as superoxide radical anion ($^{\bullet}O_2^-$) and are also particularly susceptible to oxidative damage caused by accumulation of such species.[52] This can affect mitochondrial components such as, electron transport complexes, mitochondrial DNA, proteins and membrane, potentially leading to dysfunction and cell death.[53] Notably, at low concentrations ROS species are also thought to be involved in redox signaling.[54] Further, constant exposure to accumulated ROS can be compensated to a degree by an antioxidant defence system to maintain redox balance. Cellular antioxidants include enzymes such as superoxide dismutase (SOD) and catalase (CAT) and non-enzymatic chemical antioxidants which include vitamins C and E, and GSH.

The ability to scavenge reactive oxygen species directly is unlikely to account for the antioxidant effects ascribed to endogenous H_2S. This is due to low intracellular concentrations

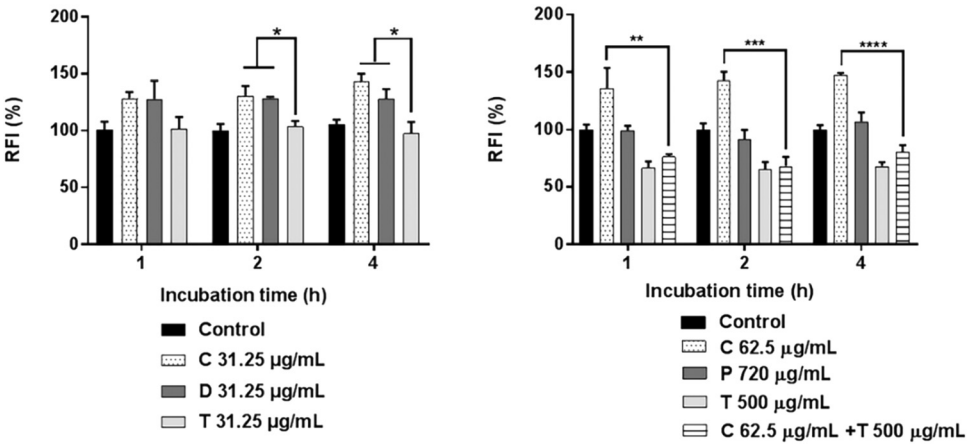

Fig. 10 ROS production in HEK293 cells treated with 31.25 µg mL^{-1} **C**, **D** and **T** (left) and **C** (62.5 µg mL^{-1}), **P** (720 µg mL^{-1}), **T** (500 µg mL^{-1}), **T** + **C** combinations (right), as measured with CellROX™ Deep Red Reagent which exhibits bright fluorescence upon oxidation by reactive oxygen species, ROS, RFI = relative fluorescence intensity *$P < 0.05$, **$P < 0.005$, ***$P < 0.001$.

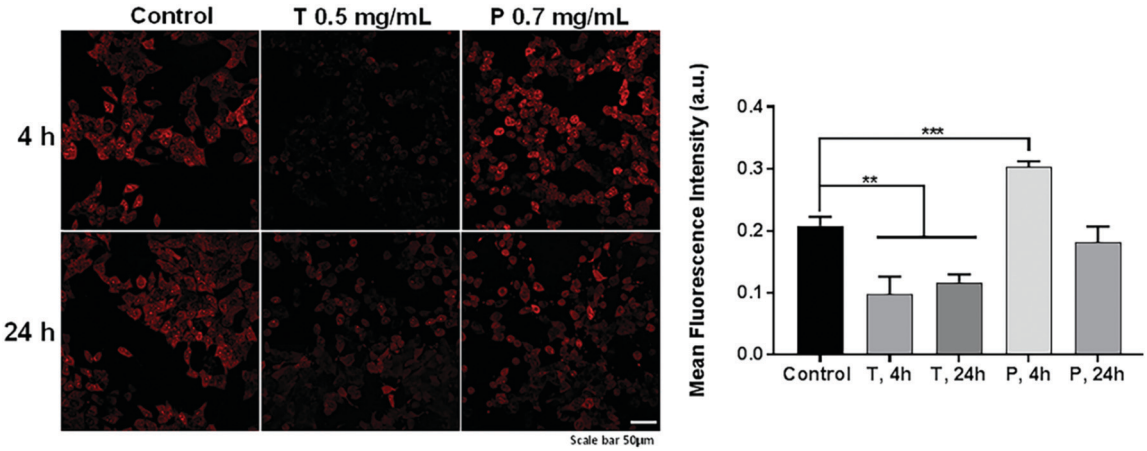

Fig. 11 Fluorescence images (left) in HEK293 cells treated with **T** (500 μg mL^{-1}) and **P** (720 μg mL^{-1}) and MitoSOX™ Red mitochondrial superoxide indicator. Fluorescence generated upon oxidation of fluorogenic dye by superoxide anion radical in the mitochondrial matrix of live cells. Quantitative mean fluorescence intensity data from images, $^{**}P < 0.005$, $^{***}P < 0.001$.

and therefore rates of reaction with ROS.[55] An emerging mechanism to explain the plethora of biological effects, including antioxidant behaviour, is the reaction of H_2S with oxidized thiols, namely protein disulfides and sulfenic acids, to form persulfides. Referred to as protein persulfidation, this post-translational modification not only alters protein function and activity but could also play a role in the protection of particular proteins from irreversible damage induced by ROS and/or reactive nitrogen species.[33]

The predominant antioxidant properties of H_2S are therefore likely brought about indirectly. Signalling occurs *via* stimulation of cellular enzymatic or non-enzymatic antioxidants, as well as various proteins responsible for inhibiting mitochondrial and membrane/cytosol ROS production. For example, H_2S was shown to increase intracellular GSH concentrations by enhancing the activity of cystine–cysteine transporters and enhancing the redistribution of GSH to mitochondria.[56] Mitochondria are thought to play a key role in cell death pathways and although various types of pro-apoptotic signals start the signaling cascade, these are thought to converge on the mitochondria.[57]

The concentrations of H_2S generated by exogenous administration (*vs.* endogenous production) may be high enough to result in direct ROS scavenging. So, this could be the case for our donors, as well as indirect antioxidant activity by stimulation of signalling proteins. However, regardless of the specific events implicated, it was of interest to us to investigate whether the ROS mitigating property of **T** was associated with mitochondria which are a major source of ROS. To enable this, we used MitoSOX™ Red mitochondrial superoxide indicator, a fluorogenic dye for selective detection of superoxide in the mitochondria of live cells. Comprised of a 3,8-diamino-5-ethyl-6-phenylphenanthridinium moiety linked by a hexyl chain to a triphenylphosphonium cation, the dye is able to be taken up by mitochondria and accumulate into the matrix in response to the negative membrane potential.[58] Referring to Fig. 11, which shows fluorescence images as well as the mean fluorescence intensity data, significantly elevated mitochondrial ROS was found to be generated by **P** *vs.* the control. Moreover, levels were found to be substantially diminished for **T** *vs.* the control after 4 hours. After 24 hours **P** only caused a minor reduction of mitochondrial ROS while **T** was able to maintain low levels of ROS *vs.* the control.

Given that **T** and **P** can release H_2S under the influence of cellular thiols, this data indicates that the cholesteryl group is an important factor involved in ROS mitigation. One possibility is that the lipid targets the H_2S release to the mitochondrial membrane or to a specific protein that is involved in ROS mitigation in the mitochondria itself. Another possibility is that the formed persulfide intermediate, CHOL-SSH, may have high propensity to react with ROS generated at the mitochondria. Although the importance of the cholesteryl group in the mitigation of ROS production is clear, further work is required to elucidate its specific role in the mediation of these biochemical processes.

Conclusions

This study involved conducting various cellular assays using HEK293 cells, exposed to four different PEG-based conjugates, either independently or in combinations with one another. By comparing the results of tests conducted on the conjugates, several unexpected aspects regarding trisulfide conjugate **T**, revealed its potential to be applied beneficially in a pharmaceutical setting:

– Using both a fluorescent probe for H_2S detection (SF4) and amperometry, the H_2S-donating ability of trisulfides, **T** and **P** was demonstrated in a cellular environment, without the need to add exogenous thiols.

– Using Alamar Blue assay, the dose-dependent effects on cell viability were tested, which showed a striking disparity in viability results between the trisulfides (**T** and **P**) and non-trisulfides (**D** and **C**). The trisulfides, **T** and **P**, showed negligible cytotoxicity, **C** showed the highest dose-dependent toxicity profile, and the results of **D** were in between. **P** was found to be well tolerated by cells, although marginally less so than **T**, to

suggest a beneficial effect on cells, by the cholesteryl group (*vs.* solely the trisulfide group).

– Using Alamar Blue assay, a cyto-protective effect was demonstrated by **T** (against **C**-induced cytotoxicity and against **D**-induced cytotoxicity). However, for **P**, a protective effect was only demonstrated against **D**, but not against **C**. These results, demonstrating cyto-protection, also support the notion that the cholesteryl group has an important role to play, and that the trisulfide group is not solely implicated. The protective effect was found for **P** (against **D**-induced toxicity *vs.* **C**-induced toxicity) is likely due to the reaction of generated H_2S with disulfides, which produces reactive persulfides, such as CHOL-SSH. These could also be pertinent mediators involved in cyto-protection as they are also produced in the case of **T**.

– Membrane effects: membrane destabilization and/or destruction are events that could take place when a self-assembled surfactant encounters cells. The CMC value of C ($\sim$13 μg mL^{-1}) indicates a tendency of **C** to interact with the membrane, whether **T** and **D**, with degradable structures and with CMC values significantly higher (67 and 90 μg mL^{-1} respectively), are less likely to do so. Membrane permeabilization does not account for the toxic effect of **C**, as demonstrated by propidium iodide test. However, by way of ratiometric imaging, using the lipophilic dye (Laurdan), membrane perturbation was instead demonstrated for **C**. Both **D** and **C** were also found to cause cells to depart from their normal cell morphology, indicating a physical interaction with the cell membrane, with potential consequences on cell viability.

– ROS generation: a comparison of ROS levels to basal levels, using a fluorescent probe for detection, showed that conjugates **C** and **D** cause an increase in ROS, **P** is ineffectual, whilst **T** causes a significant drop in ROS. Mitochondrial ROS was found to be substantially diminished for **T** *vs.* the control, especially after 4 hours.

– Overall, membrane perturbation, leading to ROS generation, are likely events that lead to cell death for conjugate **C**, which has a high tendency to self-assemble and no opportunity to degrade in a cellular environment. This contrasts with **T**, which has a much higher CMC value and a strong tendency to degrade in a cellular environment. A high capacity to reduce ROS in the mitiochondria is a likely reason for cyto-protection offered by **T**. The importance of a cholesteryl group in combination with the ability to generate H_2S was demonstrated by the superior results achieved by **T** *vs.* **P**. However, we are unable to conclude whether persulfide intermediates, such as CHOL-SSH, which are potentially generated on degradation, or H_2S itself are the mediators of such protection, however, these would be interesting factors for consideration in further studies.

Conflicts of interest

There are no conflicts to declare.

Acknowledgements

This work was carried out within the ARC Centre of Excellence in Convergent Bio-Nano Science and Technology (CE140100036). T. P. Davis is grateful for the award of an Australian Laureate Fellowship from the ARC (FL140100052) and J. F. Quinn for an ARC Future Fellowship (FT170100144). The authors acknowledge support from the Australian Research Council (DP170102950) and the Monash University Institute of Pharmacy and Pharmaceutical Sciences (MIPS).

Notes and references

1 E. C. Estevam, L. Faulstich, S. Griffin, T. Burkholz and C. Jacob, *Curr. Org. Chem.*, 2016, **20**, 211–217.
2 R. Steudel, *Chem. Rev.*, 2002, **102**, 3905–3945.
3 P. W. Ford, M. R. Narbut, J. Belli and B. S. Davidson, *J. Org. Chem.*, 1994, **59**, 5955–5960.
4 U. Munchberg, A. Anwar, S. Mecklenburg and C. Jacob, *Org. Biomol. Chem.*, 2007, **5**, 1505–1518.
5 G. A. Benavides, G. L. Squadrito, R. W. Mills, H. D. Patel, T. S. Isbell, R. P. Patel, V. M. Darley-Usmar, J. E. Doeller and D. W. Kraus, *Proc. Natl. Acad. Sci. U. S. A.*, 2007, **104**, 17977–17982.
6 Z. Wei and B. H. S. Lau, *Nutr. Res.*, 1998, **18**, 61–70.
7 R. Wang, *Physiol. Rev.*, 2012, **92**, 791–896.
8 L. Li, P. Rose and P. K. Moore, in *Ann. Rev. Pharmacol. Toxicol.*, ed. A. K. Cho, 2011, vol. 51, pp. 169–187.
9 J. V. R. Medeiros, V. H. Bezerra, A. S. Gomes, A. L. R. Barbosa, R. C. P. Lima, P. M. G. Soares, G. A. C. Brito, R. A. Ribeiro, F. Q. Cunha and M. Souza, *J. Pharmacol. Exp. Ther.*, 2009, **330**, 764–770.
10 J. L. Wallace, M. Dicay, W. McKnight and G. R. Martin, *FASEB J.*, 2007, **21**, 4070–4076.
11 X. L. Wang, Q. Wang, W. Guo and Y. Z. Zhu, *Biosci. Rep.*, 2011, **31**, 87–98.
12 S. Jha, J. W. Calvert, M. R. Duranski, A. Ramachandran and D. J. Lefer, *Am. J. Physiol. Heart Circ. Physiol.*, 2008, **295**, H801–H806.
13 D.-D. Wu, D.-Y. Wang, H.-M. Li, J.-C. Guo, S.-F. Duan and X.-Y. Ji, *Oxid. Med. Cell Longev.*, 2019, 3831713.
14 K. Qu, S. W. Lee, J. S. Bian, C. M. Low and P. T. H. Wong, *Neurochem. Int.*, 2008, **52**, 155–165.
15 H. Kimura, Y. Nagai, K. Umemura and Y. Kimura, *Antioxid. Redox Signaling*, 2005, **7**, 795–803.
16 K. Chegaev, B. Rolando, D. Cortese, E. Gazzano, I. Buondonno, L. Lazzarato, M. Fanelli, C. M. Hattinger, M. Serra, C. Riganti, R. Fruttero, D. Ghigo and A. Gasco, *J. Med. Chem.*, 2016, **59**, 4881–4889.
17 J. L. Wallace, G. Caliendo, V. Santagada, G. Cirino and S. Fiorucci, *Gastroenterology*, 2007, **132**, 261–271.
18 B. Geng, L. Chang, C. Pan, Y. Qi, J. Zhao, Y. Pang, J. Du and C. Tang, *Biochem. Biophys. Res. Commun.*, 2004, **318**, 756–763.
19 H. Wei, R. Zhang, H. Jin, D. Liu, X. Tang, C. Tang and J. Du, *Antioxid. Redox Signaling*, 2010, **12**, 1079–1091.
20 H. Yao, S. Luo, J. Liu, S. Xie, Y. Liu, J. Xu, Z. Zhu and S. Xu, *Chem. Commun.*, 2019, **55**, 6193–6196.
21 Z. L. Yang, C. T. Yang, L. C. Xiao, X. X. Liao, A. P. Lan, X. Y. Wang, R. X. Guo, P. X. Chen, C. H. Hu and J. Q. Feng, *Int. J. Mol. Med.*, 2011, **28**, 397–403.

22 C. M. Levinn, M. M. Cerda and M. D. Pluth, *Acc. Chem. Res.*, 2019, **52**, 2723–2731.
23 Y. Zhao, A. K. Steiger and M. D. Pluth, *J. Am. Chem. Soc.*, 2019, **141**, 13610–13618.
24 U. Hasegawa and A. van Der Vlies, *Bioconjugate Chem.*, 2014, **25**, 1290.
25 J. C. Foster, S. C. Radzinski, X. Zou, C. V. Finkielstein and J. B. Matson, *Mol. Pharmaceutics*, 2017, **14**, 1300.
26 Z. Xiao, T. Bonnard, A. Shakouri-Motlagh, R. A. L. Wylie, J. Collins, J. White, D. E. Heath, C. E. Hagemeyer and L. A. Connal, *Chem. – Eur. J.*, 2017, **23**, 11294–11300.
27 M. C. Urquhart, F. Ercole, M. R. Whittaker, B. Boyd, T. P. Davis and J. F. Quinn, *Polym. Chem.*, 2018, **9**, 4431–4439.
28 L. A. Connal, *J. Mater. Chem. B*, 2018, **6**, 7122–7128.
29 M. M. Cerda, M. D. Hammers, M. S. Earp, L. N. Zakharov and M. D. Pluth, *Org. Lett.*, 2017, **19**, 2314–2317.
30 D. Liang, H. X. Wu, M. W. Wong and D. J. Huang, *Org. Lett.*, 2015, **17**, 4196–4199.
31 N. E. Francoleon, S. J. Carrington and J. M. Fukuto, *Arch. Biochem. Biophys.*, 2011, **516**, 146–153.
32 C. L. Bianco, T. Akaike, T. Ida, P. Nagy, V. Bogdandi, J. P. Toscano, Y. Kumagai, C. F. Henderson, R. N. Goddu, J. Lin and J. M. Fukuto, *Br. J. Pharmacol.*, 2019, **176**, 671–683.
33 J. Zivanovic and M. R. Filipovic, *Biochemistry*, 2016, **38**, 12–17.
34 A. K. Mustafa, M. M. Gadalla, N. Sen, S. Kim, W. Mu, S. K. Gazi, R. K. Barrow, G. Yang, R. Wang and S. H. Snyder, *Sci. Signaling*, 2009, **2**, ra72.
35 E. Cuevasanta, M. Lange, J. Bonanata, E. L. Coitino, G. Ferrer-Sueta, M. R. Filipovic and B. Alvarez, *J. Biol. Chem.*, 2015, **290**, 26866–26880.
36 M. R. Filipovic, J. Zivanovic, B. Alvarez and R. Banerjee, *Chem. Rev.*, 2018, **118**, 1253–1337.
37 E. Cuevasanta, M. N. Möller and B. Alvarez, *Arch. Biochem. Biophys.*, 2017, **617**, 9–25.
38 F. Ercole, M. R. Whittaker, M. L. Halls, B. J. Boyd, T. P. Davis and J. F. Quinn, *Chem. Commun.*, 2017, **53**, 8030–8033.
39 A. B. Sullivan and K. Boustany, *Int. J. Sulfur Chem., Part A*, 1971, **1**, 207–210.
40 V. S. Lin, A. R. Lippert and C. J. Chang, *Proc. Natl. Acad. Sci. U. S. A.*, 2013, **110**, 7131–7135.
41 J. Aguiar, P. Carpena, J. A. Molina-Bolivar and C. C. Ruiz, *J. Colloid Interface Sci.*, 2003, **258**, 116–122.
42 F. Ercole, F. M. Mansfeld, M. Kavallaris, M. R. Whittaker, J. F. Quinn, M. L. Halls and T. P. Davis, *Biomacromolecules*, 2016, **17**, 371–383.
43 D. M. Owen, C. Rentero, A. Magenau, A. Abu-Siniyeh and K. Gaus, *Nat. Protoc.*, 2012, **7**, 24–35.
44 A. S. Inacio, K. A. Mesquita, M. Baptista, J. Ramalho-Santos, W. L. C. Vaz and O. V. Vieira, *PLoS One*, 2011, **6**, 1–15.
45 R. Ernst and J. Arditti, *Toxicology*, 1980, **15**, 233–242.
46 K. Jahan, S. Balzer and P. Mosto, in *Environmental Toxicology II*, ed. A. Kungolos and M. Zamorano, 2008, vol. 110, pp. 281–290.
47 A. Perani, C. Gerardin, G. Stacey, M. R. Infante, P. Vinardell, L. Rodehuser, C. Selve and M. Maugras, *Amino Acids*, 2001, **21**, 185–194.
48 F. Ercole, M. R. Whittaker, J. F. Quinn and T. P. Davis, *Biomacromolecules*, 2015, **16**, 1886–1914.
49 N. Menard, N. Tsapis, C. Poirier, T. Arnauld, L. Moine, F. Lefoulon, J. M. Pean and E. Fattal, *Eur. J. Pharm. Sci.*, 2011, **44**, 595–601.
50 S. A. Sanchez, M. A. Tricerri and E. Gratton, *Proc. Natl. Acad. Sci. U. S. A.*, 2012, **109**, 7314–7319.
51 T. Parasassi, G. De Stasio, A. Dubaldo and E. Gratton, *Biophys. J.*, 1990, **57**, 1179–1186.
52 R. S. Balaban, S. Nemoto and T. Finkel, *Cell*, 2005, **120**, 483–495.
53 M. Schieber and N. S. Chandel, *Curr. Biol.*, 2014, **24**, R453–R462.
54 L. A. Sena and N. S. Chandel, *Mol. Cell*, 2012, **48**, 158–167.
55 D. Benchoam, E. Cuevasanta, M. N. Moller and B. Alvarez, *Antioxidants*, 2019, **8**(48), 1–23.
56 Y. Kimura, Y. I. Goto and H. Kimura, *Antioxid. Redox Signaling*, 2010, **12**, 1–13.
57 E. Murphy and C. Steenbergen, *Annu. Rev. Physiol.*, 2007, **69**, 51–67.
58 K. M. Robinson, M. S. Janes, M. Pehar, J. S. Monette, M. F. Ross, T. M. Hagen, M. P. Murphy and J. S. Beckman, *Proc. Natl. Acad. Sci. U. S. A.*, 2006, **103**, 15038–15043.

